

Hybrid atomistic simulation of fluid uptake in a deformable solid

Mahyar M. Moghadam and J. M. Rickman

Department of Materials Science and Engineering, Lehigh University, Bethlehem, Pennsylvania 18015, USA

(Received 12 October 2013; published 13 January 2014)

Fluid imbibition via diffusion in a deformable solid results in solid stresses that may, in turn, alter subsequent fluid uptake. To examine this interplay between diffusional and elastic fields, we employed a hybrid Monte Carlo–molecular dynamics scheme to model the coupling of a fluid reservoir to a deformable solid, and then simulated the resulting fluid permeation into the solid. By monitoring the instantaneous structure factor and solid dimensions, we were able to determine the compositional strain associated with imbibition, and the diffusion coefficient in the Fickian regime was obtained from the time dependence of the fluid uptake. Finally, for large, mobile fluid atoms, a non-Fickian regime was highlighted and possible mechanisms for this behavior were identified.

DOI: [10.1103/PhysRevE.89.012305](https://doi.org/10.1103/PhysRevE.89.012305)

PACS number(s): 83.10.Mj, 82.56.Lz, 62.20.dq

I. INTRODUCTION

The behavior of a matrix under fluid infiltration is of significance for designing new materials in various applications ranging from analytical separations to drug delivery. For a compliant matrix, the distortion that attends fluid uptake can lead, for example, to swelling in polymeric systems and concomitant non-Fickian diffusive behavior [1–3]. For the particular case in which the fluid permeates a porous solid and generates stresses that couple with the fluid concentration field, the resulting poroelastic response can alter the kinetic and structural response of the system [4,5]. While the conceptual framework for poroelasticity was developed in the early work of Biot [6], the field remains active given the technological relevance of this phenomenon.

Several approaches exist for modeling fluid imbibition in a system. For example, Gelb and Hopkins [7] used molecular dynamics simulation to study the dynamics of fluid flow into empty cylindrical pores in which the pore-wall atoms were immobile. Ahadian *et al.* subsequently simulated imbibition of a simple fluid into a nanochannel using atomistic simulation to investigate the wall-fluid interaction [8]. More recently, Joly [9] employed molecular dynamics (MD) simulation to examine water uptake by a carbon nanotube, and Stukan *et al.* [10] also used MD to investigate the role of nanopore roughness on fluid imbibition. As in the work of Gelb and Hopkins [7], the atoms comprising the pore walls were static. At longer length scales, a phase-field model was developed to investigate fluid infiltration in a weakly anisotropic, poroelastic solid. It was found that imbibition depended on the strength of the anisotropy and the relative orientation of the propagating fluid front [11,12].

Given the inherent computational demands of simulating fluid imbibition at the atomic scale, most such simulations of this process take the matrix atoms to be immobile. This assumption is often justified, especially for fluid atoms having small radii, in situations where elastic energy considerations are relatively unimportant. The modeling of elastic deformation that attends fluid uptakes necessitates, however, the incorporation of matrix stresses via the inclusion of matrix-atom coordinates. As an illustration of a simple system that exhibits coupling between diffusional and elastic fields, we explore in this paper the impact of elastic deformation, as described by a

compositional strain, on fluid uptake in a face-centered cubic solid that is in contact with a reservoir. Our aim is to explore the consequences of this coupling on the elastic response of the solid and the diffusional transport of the permeating fluid. For this purpose, we have tailored a hybrid Monte Carlo–molecular dynamics scheme to model fluid uptake in the solid from a reservoir that is maintained at a constant chemical potential for the fluid species. In particular, a grand-canonical Monte Carlo (GCMC) simulation is employed to maintain a fixed chemical potential in a reservoir of fluid atoms that is in contact with a solid. The trajectories of both fluid and solid atoms in the solid are obtained using MD simulation. By monitoring the fluid uptake, as well as the instantaneous structure factor and lattice parameter for the solid, we develop a description of fluid permeation in a deformable medium.

This paper is organized as follows. In Sec. II we provide some background material for this work, including a discussion of compositional strain in this context. In Sec. III, the simulation procedure is outlined, while in Sec. IV we present our simulation results. Section V contains a summary and discussion of our findings, and Sec. VI contains some conclusions.

II. BACKGROUND

A. Fluid uptake

Our analysis of fluid uptake, $M(t)$, at time t begins with a comparison to ideal, Fickian imbibition, defined here as uptake following the standard diffusion equation with a *constant* diffusion coefficient, D .

Consider a spatially uniform, solid slab confined to the region $-\ell \leq z \leq \ell$ having a diffusant concentration, $c(z, t)$, that is in contact with a diffusant (fluid) reservoir at its boundaries, $z = \pm\ell$. For the case in which $c(z, t = 0) = 0$ in the slab and $c(z = \pm\ell, t) = c_0$, one finds that [13]

$$\frac{M_F(t)}{M_\infty} = 1 - \sum_{n=0}^{\infty} \frac{8}{(2n+1)^2\pi^2} \exp\left(-\frac{D(2n+1)^2\pi^2 t}{4\ell^2}\right), \quad (1)$$

where M_∞ is the uptake at saturation (i.e., $t = \infty$) and the superscript “F” denotes Fickian behavior (i.e., following from the standard diffusion equation).

Thus, systems characterized by the uptake function given by Eq. (1) are, by our definition, Fickian in nature, and we are especially interested here in characterizing any deviations from this behavior observed in our simulations. Such deviations may occur for various reasons, including, for example, stress generation in the matrix and time-dependent structural changes (e.g., in polymers) [14,15]. In the context of this work, it is expected that the permeation of relatively large diffusant atoms in an elastic solid will generate stresses that will impede further diffusion. A link between the spatiotemporal evolution of $c(z,t)$ and generated self-stresses is described below.

B. Compositional strain

The diffusion of fluid atoms through the void space in a crystalline solid leads to self-stress, and therefore local strains, that depend on $c(z,t)$. If the reference state of the system is associated with a uniform concentration \bar{c} , then, in a cubic system, one can specify the components of the compositional strain tensor as $\epsilon_{ij}^c = \eta(c - \bar{c})\delta_{ij}$ [16]. For small strain, the corresponding stress is proportional to the elastic strain and so, in the absence of an external stress,

$$\sigma_{ij} = C_{ijkl} (\epsilon_{kl} - \epsilon_{kl}^c), \quad (2)$$

where σ_{ij} are the components of the stress tensor and C_{ijkl} are the components of the elastic constant tensor.

For a cubic solid one can readily obtain the pressure, P , in terms of the compositional strain. Taking the trace of both sides of Eq. (2) and noting that $P = -(1/3)\sigma_{ii}$ (with the summation convention), one finds that

$$P = B [3\eta(c - \bar{c}) - \epsilon_{ii}], \quad (3)$$

where B is the bulk modulus. For cases in which the pressure in the reference state is nonzero, $B = B^0 + \frac{P}{3}$. Equation (3) can be used to determine the compositional strain in a simulation from a knowledge of the bulk modulus of a material and its dimensional changes resulting from the permeation of a fluid. One aim of this paper is to relate $M(t)$ to η .

III. SIMULATION METHODOLOGY

A hybrid Monte Carlo–molecular dynamics scheme was employed here to model the coupling of a fluid reservoir to a deformable solid. From a number of such approaches developed in recent years [17–20], we selected a methodology for this study that is an extension of an earlier scheme that is well suited to the study of fluid uptake [17]. Our simulations are based on a layered geometry wherein, initially, a face-centered cubic (fcc) solid slab comprising N_s atoms of radius R_s is in contact with a fluid “reservoir” [21] containing N_f atoms of radius R_f , as shown in Fig. 1(a). The system is subject to periodic boundary conditions in each principal direction. The chemical potential of the reservoir, μ_{res} , is held fixed using GCMC (see below), and so the number of fluid atoms in the reservoir fluctuates during the course of a simulation.

The interactions in this binary system are governed by a modified Lennard-Jones potential developed by Broughton

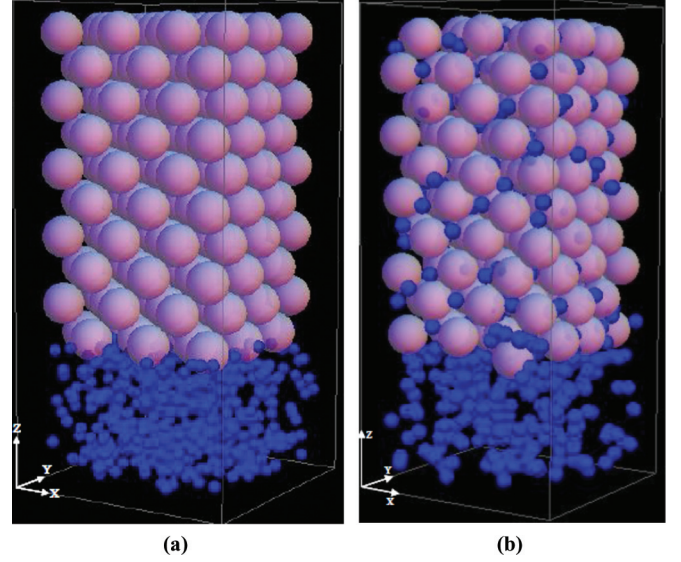


FIG. 1. (Color online) (a) A schematic of the simulation cell used to simulate fluid uptake from a reservoir into a deformable solid. (b) A snapshot showing fluid atoms dissolved in the solid.

and Gilmer [22]. The interatomic potential is given by

$$\begin{aligned} U^{\alpha\beta}(r) &= 4\epsilon^{\alpha\beta} \left[\left(\frac{\sigma^{\alpha\beta}}{r} \right)^{12} - \left(\frac{\sigma^{\alpha\beta}}{r} \right)^6 \right] + C_1, \quad r \leq 2.3\sigma^{\alpha\beta} \\ &= C_2 \left(\frac{\sigma^{\alpha\beta}}{r} \right)^{12} + C_3 \left(\frac{\sigma^{\alpha\beta}}{r} \right)^6 + C_4 \left(\frac{r}{\sigma^{\alpha\beta}} \right)^2 + C_5, \\ &\quad 2.3\sigma^{\alpha\beta} < r < 2.5\sigma^{\alpha\beta} \\ &= 0, \quad r \geq 2.5\sigma^{\alpha\beta}, \end{aligned} \quad (4)$$

where $\epsilon^{\alpha\beta}$ and $\sigma^{\alpha\beta}$ are the usual energy and length parameters, respectively, and α and β denote atom types (i.e., solid or fluid) [23]. The energy and length parameters were calculated using the Lorentz-Berthelot mixing rules, $\sigma^{\alpha\beta} = 0.5(\sigma^{\alpha\alpha} + \sigma^{\beta\beta})$, $\epsilon^{\alpha\beta} = \sqrt{\epsilon^{\alpha\alpha}\epsilon^{\beta\beta}}$. To express our results in reduced units, we take $\epsilon^{ss} = \epsilon = 1$ and $\sigma^{ss} = \sigma = 1$ where s (f) denotes solid (fluid) atoms. The other potential parameters are given, in units of ϵ , by $C_1 = 0.016132$, $C_2 = 3136.6$, $C_3 = -68.069$, $C_4 = -0.083312$, and $C_5 = 0.74689$.

A simulation begins with $N_s = 180$ solid atoms and $N_f = 170$ or $N_f = 200$ fluid atoms, with masses $m_s = 1$ and $m_f = 0.5$, in a simulation cell of fixed volume with dimensions $l \times l \times L$, where $l = 4.7\sigma$ and $L = 11.0\sigma$, in the x , y , and z directions, respectively. The solid atoms constitute a fcc crystal with a lattice parameter chosen to yield zero pressure for an isolated crystal at the desired temperature, T , using the results of Broughton and Gilmer [22]. These authors performed a series of constant-volume molecular dynamics runs in which the lattice parameter was varied from run to run to obtain zero pressure.

As fluid atoms diffuse into the solid, the solid is strained tetragonally, and therefore the volume of the fluid reservoir decreases correspondingly, consistent with a fixed simulation cell volume. A driving force for diffusion is created by maintaining the chemical potential of the fluid atoms in the

reservoir at a fixed value, μ_{res} . For this purpose, we adapted the approach of Heffelfinger and van Swol [17], who combined GCMC simulation with an isothermal molecular dynamics simulation to fix μ_{res} while allowing for diffusional transport on long time scales.

Our procedure, after setting up the simulation system, is as follows. First, fluid atoms in the reservoir are equilibrated with the conventional metropolis Monte Carlo method at fixed N_f . Then the chemical potential of the equilibrated reservoir, μ_{res} , is determined by using Widom's method [24]. Next, the system is evolved for 50 steps, with each time step being 0.005 (reduced units), using isothermal MD. Temperature control was achieved via velocity rescaling at every time step. Following this step, the chemical potential of the reservoir is readjusted to μ_{res} by applying GCMC algorithm [17], with approximately 50 attempts for atomic insertion or deletion [25]. Widom's method is used periodically to verify that the chemical potential has been set correctly. This sequence of steps is repeated until the solid is saturated with fluid atoms. Depending upon the magnitude of R_f/R_s , typical runs consisted of approximately 2×10^5 to 4×10^6 MDS. Finally, to obtain statistically meaningful data, simulation

results were averaged over many realizations of the system (typically 60–80 runs).

IV. RESULTS

The transport behavior of a fluid in a deformable solid was modeled using two different atomic size ratios, namely $R_f/R_s = 0.30$ and 0.414, to explore the impact of elastic deformation on diffusion. As both ratios are much less than one, it is expected that fluid atoms will dissolve into the interstitial voids in the fcc structure, though preferentially into the larger octahedral voids for the larger fluid atoms. Figure 1(b) shows a snapshot of the atomic coordinates after some elapsed time that highlights the dissolution of the fluid atoms.

Consider first a system with $R_f/R_s = 0.30$ at temperature $T = 0.3$. Figure 2(a) shows the uptake function, $M(t)/M_\infty$, as a function of square root of simulation time, \sqrt{t} , where time is measured in units of Δt . As expected, fluid uptake increases monotonically with time until saturation at late times. To facilitate the interpretation of these data, the uptake curve is replotted in Fig. 2(b) as a function of scaled time, \sqrt{Dt}/ℓ . The diffusion coefficient, D , was determined by fitting the Fickian uptake given in Eq. (1) to the data. More specifically, we define a parameter $\chi^2 = \sum_i [(M(t_i)/M_\infty) - (M^F(t_i)/M_\infty)]^2$,

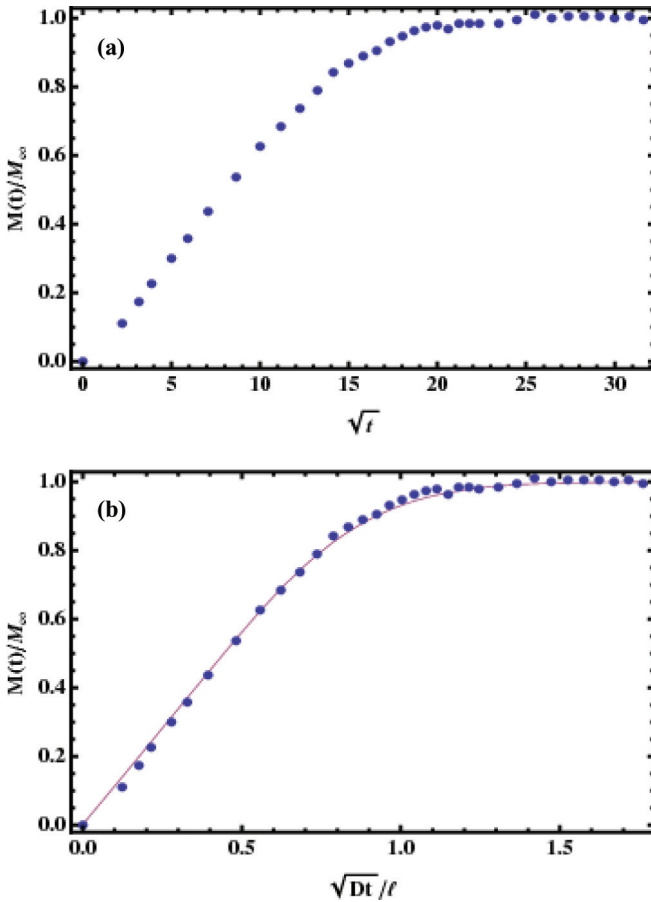


FIG. 2. (Color online) (a) The uptake function, $M(t)/M_\infty$, as a function of the square root of time, \sqrt{t} , for $R_f/R_s = 0.30$. The results were averaged over 60 independent runs with mean fractional error of 0.074 at each recorded time step. (b) The uptake function vs scaled time, \sqrt{Dt}/ℓ in comparison with the corresponding Fickian uptake function from Eq. (1) (solid line).

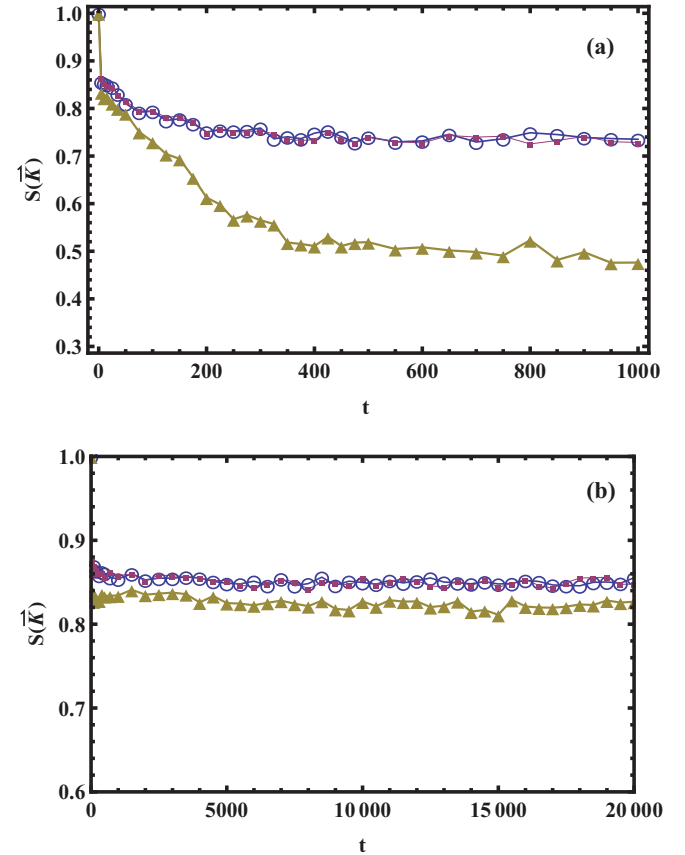


FIG. 3. (Color online) (a) The instantaneous structure factor, $S(\vec{k}, t)$, vs time for the wave vectors $\vec{k} = (4\pi/a)\hat{x}$ (\circ), $(4\pi/a)\hat{y}$ (\blacksquare), and $(4\pi/a)\hat{z}$ (\triangle), respectively, for $R_f/R_s = 0.30$. (b) The same as in panel (a), except that $R_f/R_s = 0.414$.

where the sum is over simulation times and the superscript “F” denotes the Fickian result [Eq. (1)]. The coefficient D is chosen to minimize χ^2 . For this system it was found that $D = 0.154\sqrt{\epsilon\sigma^2/m}$. For comparison, the corresponding Fickian uptake function, $M^F(t_i)/M_\infty$, is also displayed in Fig. 2(b). As is evident from the figure, the simulation data is well described by a Fickian profile, as might be expected for particles that are able to fit readily into interstices.

While the fluid particles can be accommodated by the voids in the solid, there is, nevertheless, an expansion of the solid due to the compositional strain that attends fluid permeation. To highlight this expansion and also confirm that the solid remains intact, one can calculate the instantaneous structure factor, $S(\vec{k}, t)$, for the solid atoms for a few fcc reciprocal lattice vectors. Figure 3(a) shows $S(\vec{k}, t)$ versus time for $\vec{k} = (4\pi/a)\hat{x}$, $(4\pi/a)\hat{y}$, and $(4\pi/a)\hat{z}$, where a is the lattice parameter. The relatively large values for these quantities indicate that the lattice remains intact, and the tetragonal strain in the z directions splits their degeneracy. In other words, the structure factors in Fig. 3 show that the solid lattice, while distorted due to the presence of interstitials, remains crystalline. Moreover, the smaller value of $S(\vec{k} = (4\pi/a)\hat{z}, t)$ at late times indicates that the solid is lengthening in the z direction.

A more direct measure of expansion is given in Fig. 4(a), which shows the strain component $\epsilon_{zz}(t)$ as a function of time. Clearly, ϵ_{zz} increases with time until saturation as the simulation cell expands to accommodate fluid atoms. The

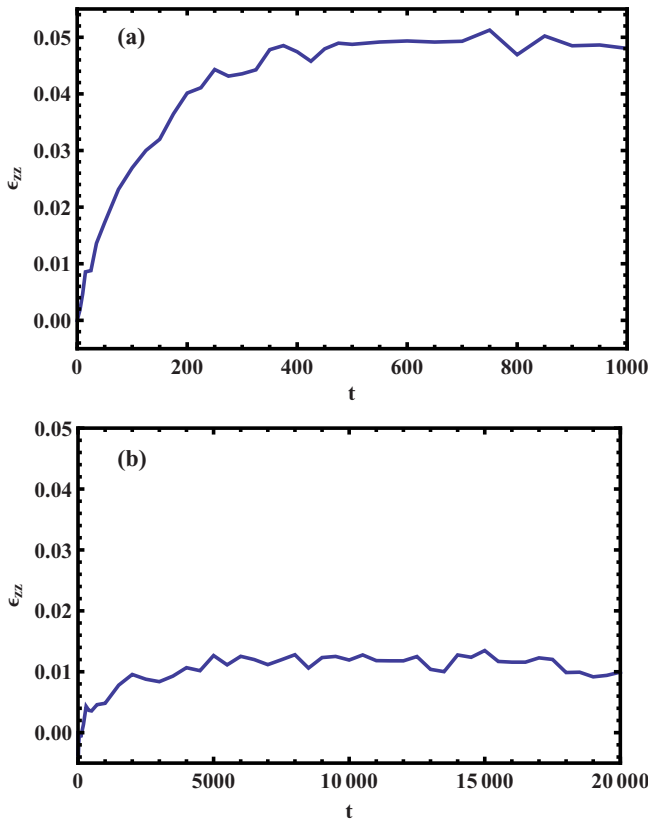


FIG. 4. (Color online) (a) The tetragonal strain component, $\epsilon_{zz}(t)$, vs time for $R_f/R_s = 0.30$ and $R_f/R_s = 0.414$, respectively. (b) The same as in panel (a), except that $R_f/R_s = 0.414$.

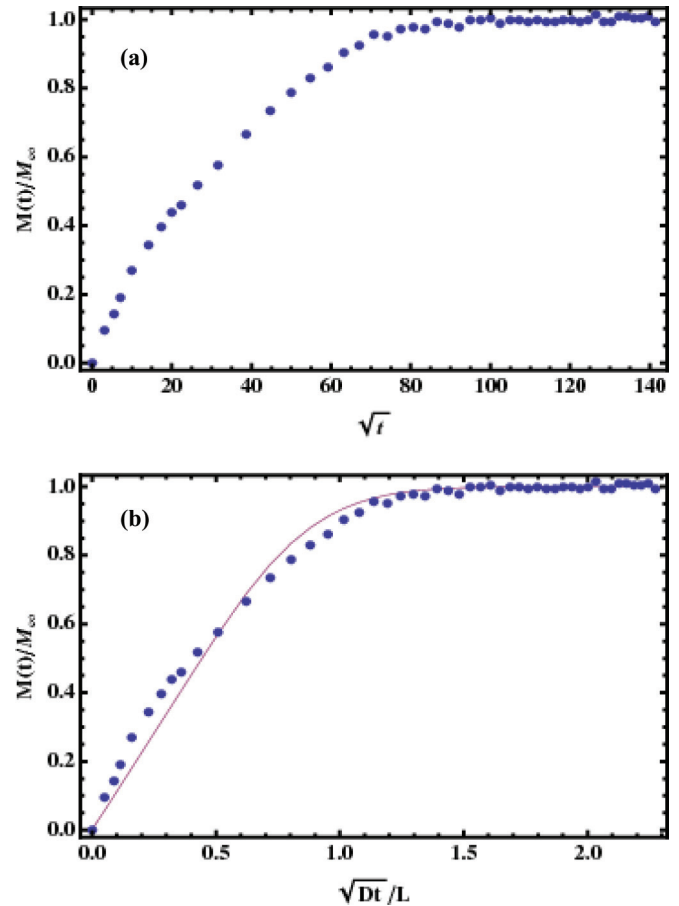


FIG. 5. (Color online) (a) The uptake function, $M(t)/M_\infty$, as a function of the square root of time, \sqrt{t} , for $R_f/R_s = 0.414$. The results were averaged over 80 independent runs with mean fractional error of 0.107 at each recorded time step. (b) The uptake function vs scaled time, \sqrt{Dt}/l in comparison with the corresponding Fickian uptake function from Eq. (1) (solid line).

value of the strain at saturation, $\epsilon_{zz} \approx 0.05$, can be used to determine the associated compositional strain parameter η using Eq. (3). At this temperature, the bulk modulus $B = 45.8\epsilon/\sigma^3$ and so, given the calculated pressure at saturation, one finds that $\eta = 0.02$.

Consider next a system with $R_f/R_s = 0.414$, again held at temperature $T = 0.3$. Figure 5(a) shows the uptake function, $M(t)/M_\infty$, as a function of square root of simulation time, \sqrt{t} , and Fig. 5(b) shows the uptake function and the corresponding Fickian uptake function versus \sqrt{Dt}/l . As before, the value for D was determined from a best fit using the χ^2 parameter, and the compositional strain parameter $\eta = 0.04$ was determined from ϵ_{zz} at saturation [see Fig. 4(b)], as above, by using Eq. (3). As is evident from the figure, the uptake function is not accurately described by the Fickian uptake function. The origin of this non-Fickian behavior is discussed below.

The strain is, of course, associated with diffusant atoms distorting the local atomic environment around structural voids. These local distortions are reflected in $S(\vec{k}, t)$, as displayed in Fig. 3(b), for the same high-symmetry reciprocal lattice vectors used above. The tetragonal strain induced in the z direction again splits the degeneracy in the structure factor,

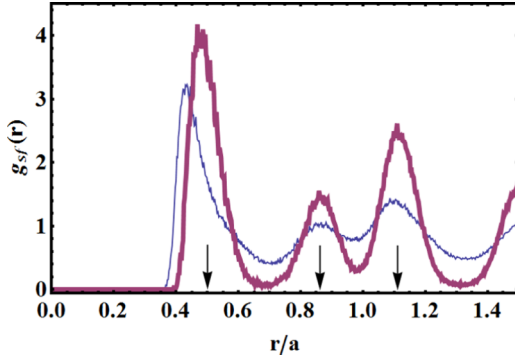


FIG. 6. (Color online) The partial radial distribution function, $g_{sf}(r)$, vs distance, r where s and f denote the solid and fluid species, respectively, for $R_f/R_s = 0.30$ (thin curve) and $R_f/R_s = 0.414$ (thick curve). The arrows indicate the location of octahedral interstices. Note that the peaks corresponding to the octahedral locations are more pronounced for $R_f/R_s = 0.414$.

the relatively large value of $S(\vec{k} = (4\pi/a)\hat{z}, t)$, due to the fact that large interstitials constrain the vibrations of lattice atoms. The spatial distribution of the fluid atoms in the available interstices is highlighted in Fig. 6, which shows the partial radial distribution function, $g_{sf}(r)$, versus distance, r , where s (f) denotes the solid (fluid) atoms, for both $R_f/R_s = 0.30$ and $R_f/R_s = 0.414$. In principle, diffusant atoms can reside in either octahedral or tetrahedral interstices, though larger elastic strains (and therefore a larger strain energy) are associated with the tetrahedral voids. However, as noted from the figure, the peaks corresponding to the octahedral voids (indicated by the positions of the arrows) become more pronounced for $R_f/R_s = 0.414$ as these larger voids are required to accommodate larger atoms.

V. DISCUSSION

As noted above, the normalized uptake function for a diffusant with $R_f/R_s = 0.414$ is not well described by the corresponding Fickian uptake function given in Eq. (1). There are at least two possible reasons for this disagreement. First, in stressed solids, the chemical potential is a function of both concentration and stress (i.e., $\mu = \mu(c, \sigma_{ij})$), and therefore the diffusive flux is, in general, a function of the stress state of the system. For cases in which diffusing atoms are relatively large, the flux will depend on the resulting self-stresses and therefore η . In some cases this stress dependence leads to a flux that depends on the concentration throughout the system, rather than simply on the gradient of the local concentration. In the appendix we discuss in more detail the role of self-stress on diffusion in our problem. It is found that, in our case, the flux depends only on the gradient of the local concentration, and the corresponding diffusion equation is therefore spatially local. Thus, the dependence of the driving force for diffusion on stress does not explain the observed behavior of the uptake function.

Another possible reason for the observed non-Fickian behavior is that the diffusion coefficient is a function of the local concentration, c , as might be expected for interacting diffusant atoms [26]. Such interactions arise from the interatomic

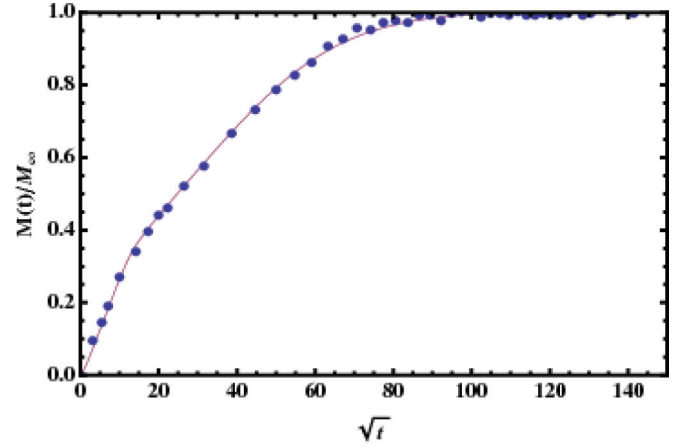


FIG. 7. (Color online) The uptake function, $M(t)/M_\infty$, as a function of the square root of the simulation time, \sqrt{t} , for $R_f/R_s = 0.414$. Also shown is the uptake as calculated using Eqs. (5) and (6) (solid line).

potential and from the elastic coupling of centers of dilatation moving in an anisotropic medium. Thus, in our system, one would expect diffusive motion to occur readily for c small, but to become slower for larger c as stresses generated by the diffusant atoms constrict interstices and migration pathways. To examine this possibility, we consider a simple, two-step parametrization of the diffusion coefficient, namely

$$D(c) = D_1(\eta)\Theta(c) - D_2(\eta)\Theta[c - c_0(\eta)], \quad 0 \leq c \leq 1, \quad (5)$$

where D_1 , D_2 , and c_0 are constants that depend on the compositional strain parameter η and θ denotes the unit step function.

For this parametrization, we solved the associated one-dimensional diffusion equation

$$\frac{\partial c}{\partial t} = \frac{\partial}{\partial z} \left(D(c) \frac{\partial c}{\partial z} \right) \quad (6)$$

numerically using the method of lines [27] for our thin-slab geometry. The corresponding uptake function is displayed in Fig. 7, along with the simulation results, for the choices $D_1 = 0.11\sqrt{\epsilon\sigma^2/m}$, $D_2 = 0.01\sqrt{\epsilon\sigma^2/m}$, and $c_0 = 0.2$. This simplified parametrization of $D(c)$ is seen to provide a good description of the simulation results. From these considerations one can infer the behavior of these parameters as a function of η . For example, one can see that c_0 increases as η decreases, with $c_0 \rightarrow 1$ as $\eta \rightarrow 0$. In addition, it is clear that D_1 is a monotonically decreasing function of η as larger atoms are associated with greater strain along diffusive pathways.

VI. CONCLUSIONS

A hybrid Monte Carlo–molecular dynamics scheme was employed here to model the coupling of a fluid reservoir to a deformable solid, and the resulting permeation of the fluid into the solid was examined to highlight the interplay between diffusional and elastic fields. Both Fickian and non-Fickian regimes were identified and described in terms of the relative size of the fluid and solid atoms. The impact of self-stresses on solid-state diffusion were investigated by monitoring the

fluid uptake and evolving partial structure factors and radial distribution functions.

The results obtained here suggest that analogous simulation studies of fluid uptake in porous media will be useful in elucidating the roles of pore geometry and stress on diffusion. Given the geometric complexity of a porous medium, it will be of interest to characterize the interconnectivity of the porous network and to calculate the local stresses [28] in different regions of the system. It is expected that the swelling of portions of this network that attend diffusion will alter the corresponding diffusive flux. A simulational study of fluid uptake by a porous medium is the subject of future work.

ACKNOWLEDGMENTS

We acknowledge the donors of the American Chemical Society Petroleum Research Fund for support of this research under PRF No. 49139-ND8. We also thank the Minnesota Supercomputing Institute for its generous support.

APPENDIX

In this appendix, we examine the dependence of the diffusive flux on the concentration field. The diffusive flux depends on the gradient of the chemical potential of the diffusing species and, as discussed above for a deformable solid, this potential depends on the stress state of the system. With the assumption that mechanical equilibrium obtains quickly on the time scale of mass diffusion, it can be shown that in some cases the stress is a functional of the concentration field, thereby rendering diffusion spatially nonlocal and therefore non-Fickian. One such case is that of mass transport in an infinite, elastically anisotropic solid having cubic symmetry [29]. Another example is that of diffusion in an elastically isotropic plate in which one side of the plate is in contact with a fluid, with a resulting asymmetric concentration profile [16]. The system considered here is a thin, elastically anisotropic plate having cubic symmetry in contact with a fluid on two faces. We consider below the diffusive flux in this system.

Larché and Cahn [29] have shown that the components of the diffusive flux, \vec{J} , can be written as

$$J_i = -\mathcal{L} \frac{\partial}{\partial x_i} [\mu_0(c) - (\eta/\rho)\sigma_{kk}(\vec{r})], \quad (\text{A1})$$

where \mathcal{L} is a kinetic coefficient, μ_0 is a part of the chemical potential that depends on concentration, and ρ is the density. It has been assumed here that the elastic constants of the system do not depend on c .

Assuming that the elastic fields relax quickly on the time scale of atomic diffusion, σ_{ij} can be expressed in terms of c . This may be accomplished by starting with the equations of compatibility [30]

$$e_{ikr} e_{jls} \frac{\partial^2 \epsilon_{ij}}{\partial x_k \partial x_l} = 0, \quad (\text{A2})$$

where e_{ikr} are the components of the Levi-Civita tensor, and rewriting them in terms of the stress.

The components of the strain tensor can be written in terms of those of the stress tensor by inverting Eq. (2) to obtain

$$\epsilon_{ij} = S_{ijkl} \sigma_{kl} + \epsilon_{ij}^c, \quad (\text{A3})$$

where the S_{ijkl} are the components of the compliance tensor. For a cubic solid [31],

$$S_{ijkl} = \alpha \delta_{ij} \delta_{kl} + \beta (\delta_{ik} \delta_{jl} + \delta_{il} \delta_{jk}) + \gamma \delta_{ijkl}, \quad (\text{A4})$$

where δ_{ij} is the Kronecker δ and $\delta_{ijkl} = 1$ if $i = j = k = l$ and otherwise zero. Also, for this case, $\epsilon_{ij}^c = \eta (c - \bar{c}) \delta_{ij}$. The coefficients in Eq. (A4) can be written in terms of the elastic constants (in Voigt notation) as

$$\begin{aligned} \alpha &= -\frac{C_{12}}{(C_{11} - C_{12})(C_{11} + 2C_{12})}, \\ \beta &= \frac{1}{4C_{44}}, \\ \gamma &= -\frac{\tau}{2(C_{11} - C_{12})C_{44}}, \end{aligned} \quad (\text{A5})$$

where the anisotropy factor $\tau = C_{11} - C_{12} - 2C_{44}$ vanishes for an isotropic solid. Upon inserting Eqs. (A3) and (A4) into Eq. (A2) and taking a trace, one finds that

$$\begin{aligned} \nabla^2 \left[\sigma_{kk} + \left(\frac{\eta}{\alpha + \beta + \gamma/2} \right) c \right] + \left(\frac{\gamma}{2\alpha + 2\beta + \gamma} \right) \\ \times \left[\frac{\partial^2 \sigma_{11}}{\partial x_1^2} + \frac{\partial^2 \sigma_{22}}{\partial x_2^2} + \frac{\partial^2 \sigma_{33}}{\partial x_3^2} \right] = 0. \end{aligned} \quad (\text{A6})$$

For an isotropic solid, Eq. (A6) can be simplified to read

$$\nabla^2 \left[\sigma_{kk} + \left(\frac{2E\eta}{1-\nu} \right) c \right] = 0, \quad (\text{A7})$$

where E and ν are the Young's modulus and Poisson's ratio, respectively.

We first consider the isotropic case. Following Larché and Cahn [16], one has that

$$\sigma_{kk} + \left(\frac{2E\eta}{1-\nu} \right) c = Sz + T, \quad (\text{A8})$$

where S and T are constants. Since the boundary conditions for the thin slab are the same at $\pm \ell$, $S = 0$, and so $\vec{\nabla} \sigma_{kk} = -2E\eta/(1-\nu)\vec{\nabla} c$ and the flux is therefore spatially local [32].

For the case of medium with cubic anisotropy modeled here, the stresses σ_{11} and σ_{22} are independent of x and y as the system is translationally invariant in the xy plane. Moreover, since $\sigma_{31} = \sigma_{32} = 0$, a solenoidal stress implies that σ_{33} is constant and so Eq. (A6) becomes

$$\nabla^2 \left[\sigma_{kk} + \left(\frac{\eta}{\alpha + \beta + \gamma/2} \right) c \right] = 0. \quad (\text{A9})$$

Given the discussion above, one again concludes that $\vec{\nabla} \sigma_{kk}$ depends only on $\vec{\nabla} c$ and that the flux is spatially local.

- [1] D. A. Edwards, *J. Polym. Sci. B* **34**, 981 (1996).
- [2] P. Gao and M. R. Mackley, *Proc. R. Soc. London A* **444**, 267 (1994).
- [3] C.-Y. Hui, K.-C. Wu, R. Lasky, and E. J. Kramer, *J. Appl. Phys.* **61**, 5129 (1987).
- [4] H. F. Wang, *Theory of Poroelasticity with Applications to Geomechanics and Hydrology* (Princeton University Press, Princeton, NJ, 2000).
- [5] S. C. Cowin, *Transp. Porous Media* **50**, 35 (2003).
- [6] M. A. Biot, *J. Appl. Phys.* **12**, 155 (1941).
- [7] L. D. Gelb and A. C. Hopkins, *Nano Lett.* **2**, 1281 (2002).
- [8] S. Ahadian, H. Mizuseki, and Y. Kawazoe, *J. Colloid Interface Sci.* **352**, 566 (2010).
- [9] L. Joly, *J. Chem. Phys.* **135**, 214705 (2011).
- [10] M. R. Stukan, P. Ligneul, J. P. Crawshaw, and E. S. Boek, *Langmuir* **26**, 13342 (2010).
- [11] M. Dubé, M. Rost, K. R. Elder, M. Alava, S. Majaniemi, and T. Ala-Nissila, *Phys. Rev. Lett.* **83**, 1628 (1999).
- [12] J. M. Rickman, *J. Appl. Phys.* **106**, 044911 (2009).
- [13] J. Crank, *The Mathematics of Diffusion* (Oxford University Press, Oxford, 1975).
- [14] J. H. Petropoulos, M. Sanopoulou, and K. Papadokostaki, *Eur. Polym. J.* **47**, 2053 (2011).
- [15] D. De Kee, Q. Liu, and J. Hinestroza, *Can. J. Chem. Eng.* **83**, 913 (2005).
- [16] F. C. Larché and J. W. Cahn, *Acta Metallurgica* **30**, 1835 (1982).
- [17] G. S. Heffelfinger and F. van Swol, *J. Chem. Phys.* **100**, 7548 (1994).
- [18] G. C. Lynch and B. M. Pettitt, *J. Chem. Phys.* **107**, 8594 (1997).
- [19] J. Ji, T. Cagin, and B. M. Pettitt, *J. Chem. Phys.* **96**, 1333 (1992).
- [20] A. Papadopoulou, E. D. Becker, M. Lupkowski, and F. van Swol, *J. Chem. Phys.* **98**, 4897 (1993).
- [21] In this context, the reservoir has a finite extent. It is connected, via a GCMC scheme, to a particle reservoir that maintains its chemical potential.
- [22] J. Q. Broughton and G. H. Gilmer, *J. Chem. Phys.* **79**, 5095 (1983).
- [23] As is customary, the symbols ε and σ are used here for potential parameters, with superscripts to denote atom types. They should not be confused with the symbols for the components of the strain and stress, which are second-rank tensors.
- [24] B. Widom, *J. Chem. Phys.* **39**, 2808 (1963).
- [25] D. Frenkel and B. Smit, *Understanding Molecular Simulation: From Algorithms to Applications*, 2nd ed. (Academic Press, San Diego, 2001).
- [26] R. Kutner, K. Binder, and K. W. Kehr, *Phys. Rev. B* **26**, 2967 (1982).
- [27] W. E. Schiesser, *The Numerical Method of Lines: Integration of Partial Differential Equation* (Academic Press, San Diego, 1991).
- [28] J. Cormier, J. M. Rickman, and T. J. Delph, *J. Appl. Phys.* **89**, 99 (2001).
- [29] F. Larché and J. W. Cahn, *Acta Metallurgica* **33**, 331 (1985).
- [30] T. M. Atanackovic and A. Guran, *Theory of Elasticity for Scientists and Engineers* (Birkhäuser, Boston, 2000).
- [31] T. Mura, *Micromechanics of Defects in Solids* (Martinus Nijhoff, The Hague, 1982).
- [32] We note that Larché and Cahn considered the case of a slab in contact with fluid only along one face. For this case, the flux is nonlocal [16].